Journal of Laser Applications

Evaluation of narrowed weld pool shapes and their effect on resulting potential defects during deep penetration laser beam welding

Cite as: J. Laser Appl. **34**, 042005 (2022); https://doi.org/10.2351/7.0000733
Submitted: 10 June 2022 • Accepted: 21 August 2022 • Published Online: 19 September 2022

Marcel Bachmann, Xiangmeng Meng, Antoni Artinov, et al.

Journal of Laser Applications ARTICLE scitation.org/journal/jla

Evaluation of narrowed weld pool shapes and their effect on resulting potential defects during deep penetration laser beam welding

Cite as: J. Laser Appl. **34**, 042005 (2022); doi: 10.2351/7.0000733
Submitted: 10 June 2022 · Accepted: 21 August 2022 ·
Published Online: 19 September 2022

Marcel Bachmann,[1] Xiangmeng Meng,[1] Antoni Artinov,[1] and Michael Rethmeier[1,2,3]

AFFILIATIONS

[1]Bundesanstalt für Materialforschung und -prüfung (BAM), Unter den Eichen 87, 12205 Berlin, Germany
[2]Institute of Machine Tools and Factory Management, Technische Universität Berlin, Pascalstraße 8-9, 10587 Berlin, Germany
[3]Fraunhofer Institute for Production Systems and Design Technology, Pascalstraße 8-9, 10587 Berlin, Germany

Note: Paper published as part of the special topic on Proceedings of the International Congress of Applications of Lasers & Electro-Optics 2022.

ABSTRACT

This study presents mechanisms of the evolution of a narrowed region in the weld pool center during deep penetration laser beam welding. In numerous numerical studies presented in this study, it was also found that the local reduction of the weld pool size can cause detrimental effects on the melt flow behavior and the resulting properties of the welds. A particularly large influence of this effect was identified in three aspects. First, the local variation of the solidification sequence of the weld pool causes an increase in the hot-cracking susceptibility due to a locally delayed solidification. Second, it was proven that a change in the local length and width of the weld pool is associated with an adverse impact on the potential flow routes of the molten material that induces stronger local variations of its solidification. Thus, the element mixing, e.g., during the welding with filler materials, is blocked. This leads to a nonhomogeneous chemical composition of the final weld and can cause undesired effects on the final material properties. Finally, another observed effect is related to the reduced ability of process pores to reach the top surface. As this type of porosity is usually produced around the keyhole tip, the change of the fluid flow regime above this area plays a significant role in determining the final path of the pores until the premature solidification in the middle of the weld pool captures them. This study summarizes mainly numerical results that were supported by selected experimental validation results.

Key words: weld pool shape, laser beam welding, solidification, porosity, element distribution, numerical process simulation

I. INTRODUCTION

In the last decades, deep penetration laser beam welding (LBW) has made its way into many industrial applications. The main reason for that is, especially when compared to traditional, e.g., arc welding, processes, LBW offers unique advantages. The highly localized heat input can be precisely controlled, the material penetration by the laser beam allows for single-pass deep penetration welding, and the process characteristics mostly lead to superior residual distortion development. The favorable penetration capacity of the laser beam is associated with the utilization of a small laser spot and a correspondingly high energy density leading to high reachable welding depths.[1,2] On the other side, the characteristics of the deep penetration LBW process are associated with some drawbacks. These are, not exclusively, due to the small dimension of the laser spot and corresponding issues when it comes to assembly tolerances of the workpiece, the high solidification rates, and related issues regarding hot-cracking, as well as the evolution of deep and narrow weld pool geometries that are detrimental for the ability of keyhole-tip pores to escape from the melt before its final solidification.[3]

Typical weld pool shapes during deep penetration LBW are elongated at the free surfaces, that is, the upper region in partial

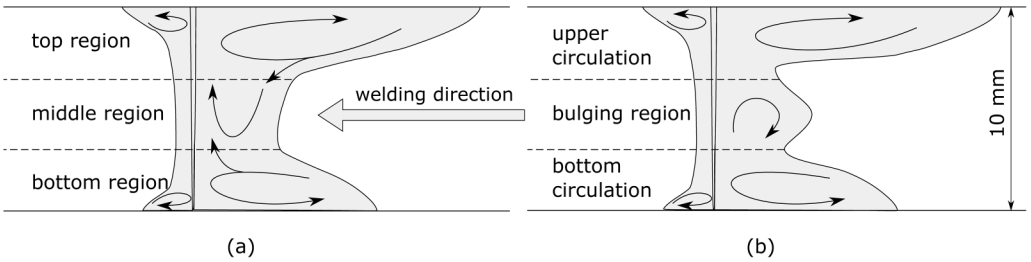

FIG. 1. Comparison of different exemplary weld pool shapes for full-penetration welding. (a) Typical weld pool shape with three-dimensional flow routes across all areas. (b) Untypical weld pool shape with narrowed region thus being disadvantageous in terms of potential vertical flow channels.

penetration welding and the upper and lower surfaces during full-penetration welding. The reason for that is the balance between the main driving forces in the weld pool, namely, the recoil pressure of the evaporating material that pushes the melt and the Marangoni shear stress at the free surfaces due to surface tension gradients. In the vertical center of the weld longitudinal section, it is relatively shorter in the bottom region or between the free surfaces, respectively,[4,5] which leads to a regular solidification sequence from the middle of the weld pool toward the free surfaces in full-penetration welding and from the bottom to the top in partial penetration welding. However, in early studies of the electron beam welding process, an internal widening of the weld pool at the solid-liquid interface was detected and associated with increased susceptibility to hot-cracking.[6,7] Another somewhat different type of molten pool shape was also observed both experimentally and numerically in recent studies.[8,9] A very typical elongation of the melt pool boundary is seen here in the upper and lower regions of the weld pool. In the middle part, the molten pool is significantly narrowed. Sometimes, this effect is accompanied by the occurrence of the bulging phenomenon with a characteristic elongation of the bottom region in partial penetration LBW or even the center part in full-penetration LBW.[10]

The effect of an untypical narrowing of the weld pool was found to play a potentially crucial role in the formation of different weld defects. On the one hand, it is obvious that common issues, especially in deep penetration LBW, such as solidification cracking and porosity can be affected by the modified flow routes in the weld pool and the associated change in the solidification behavior. On the other hand, the narrowing and also the bulge in the weld pool associated with a deteriorated potential downward transfer of the material result as well in a limited capability of alloying elements fed into the process, e.g., the filler wire during wire-based LBW processes. As a consequence, the final weld properties are nonhomogeneous and the weld quality is affected, e.g., in terms of its mechanical behavior.[11] Exemplary longitudinal weld pool shapes for full-penetration LBW can be seen in Fig. 1, and the same in the case of partial penetration welding in Fig. 2, respectively.

Since the formation of the described narrow regions in the weld pool can only be investigated experimentally with high efforts, for example, using *in situ* x-ray imaging or a welding configuration combining a metal plate and a transparent quartz glass plate, thus potentially affecting the welding process, this study aims to summarize the complicated interactions of the physical effects involved mainly by numerical simulations of heat transfer and fluid flow. For validation purposes, exemplary welding experiments were conducted, e.g., to measure weld pool dimensions and compare them to the numerical results.

II. EXPERIMENT SETUP

In this study of the narrowing phenomena in the weld pool, LBW experiments were conducted with AISI 304 stainless steel as well as different unalloyed steel grades. The material of the filler wire was the NiCr20Mo15 alloy. The size of the experimental specimen for the investigation of the filler wire dilution was 200 mm in length, 60 mm in width, and a thickness of 10 mm. The used filler wire diameter was 1.1 mm. These experiments were done using an

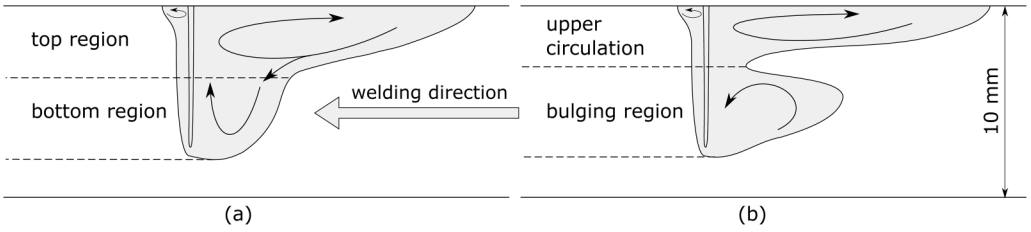

FIG. 2. Comparison of different exemplary weld pool shapes for partial penetration welding. (a) Typical weld pool shape with three-dimensional flow routes across all areas. (b) Untypical weld pool shape with the narrowed region.

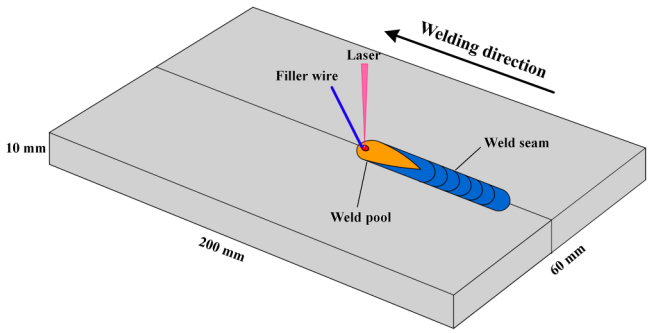

FIG. 3. Exemplary sketch for wire feed laser beam welding of 10 mm thick AISI 304 austenitic stainless steel.

IPG YLR 20000 laser system with an operational wavelength of 1.07 μm. The laser beam diameter in the focal plane, which was set 3 mm below the upper surface, was 560 μm. The laser power used was 6.5 kW, and the welding speed was 1.3 m/min. The leading filler wire angle was 33° at a feeding rate of 2.1 m/min. A sketch of the experimental setup can be seen in Fig. 3.

In addition, experiments with unalloyed steel S355 were done. For these experiments, a Trumpf laser TruDisk 16002 with a wavelength of 1.03 μm was utilized. The focal diameter was 500 μm and the focus plane was set at the workpiece surface. The specimen thicknesses were between 8 and 12 mm and the used laser power was 7.5 and 8 kW, respectively. The welding speed was 2 m/min. Argon shielding gas at a flow rate of around 20 l/min was provided.

The filler material mixing with the base material was analyzed by *ex situ* x-ray fluorescence (XRF) element mapping with a scanning spot size of 20 μm and a measurement time per spot of 50 ms. μ-CT measurements were performed to visualize the residual porosity. The samples with a scanning volume of $30 \times 6 \times 10\ \text{mm}^3$ were measured with a voltage of 215 kV and a current of 100 μA. The resolution of μ-CT was 10 μm.

III. NUMERICAL SETUP

A three-dimensional CFD model was developed being able to calculate heat transfer, fluid flow, and free surface deformation during LBW and also to account for the effects of the filler wire. All phases were assumed to be Newtonian incompressible fluids and the Reynolds number of the liquid metal during the process is assumed to be sufficiently low. Hence, a laminar solver approach was adopted for the fluid flow calculation.[12] Hexahedral mesh cells with a minimum cell size of 0.2 mm were used in the fusion zone, and the cell size grows gradually in the zone far away from the molten pool. The transport equations, the volume-of-fluid (VOF) equation, and the magnetic induction equation were solved by the CFD software ANSYS Fluent 19.5. The convection-diffusion equations were spatially discretized by the second-order upwind method. The average time step was around 1×10^{-5} s. The pressure-implicit with splitting of operators (PISO) algorithm was applied for the pressure-velocity coupling.

The free surface tracking was realized by the VOF approach[13]

$$\frac{\partial \phi}{\partial t} + \nabla \cdot (\vec{v}\phi) = S_f. \tag{1}$$

Here, t is the time and ϕ represents the volume fraction of different phases, i.e., the Ar gaseous phase and the steel phase, and S_f is the volume source term from the filler wire.

The mass conservation as well as the Navier–Stokes equations were used to describe the liquid flow in the model. These can be written as

$$\nabla \cdot \vec{v} = \frac{m_w}{\rho}, \tag{2}$$

$$\rho\left(\frac{\partial \vec{v}}{\partial t} + \vec{v} \cdot \nabla \vec{v}\right) = -\nabla p + \mu \nabla^2 \vec{v} - \mu K \vec{v} + m_w \vec{v}_w + \vec{S}_m, \tag{3}$$

where $\vec{v}$ and $\vec{v}_w$ are the velocities of the liquid metal and the molten filler material, ρ is the density, p is the pressure, μ is the dynamic viscosity, K is the Carman–Kozeny equation coefficient for the enthalpy-porosity solidification model,[14,15] and $\vec{S}_m$ is a volumetric force term including gravity, buoyancy,[16] recoil pressure,[17] surface tension, and Marangoni stress.[18]

The heat transfer was calculated according to the standard energy conservation equation

$$\rho\left[\frac{\partial h}{\partial t} + (\vec{v} \cdot \nabla)h\right] = \nabla \cdot (k \nabla T) + h_w + S_q, \tag{4}$$

with the temperature T, the thermal conductivity k, and the enthalpy h. Here, h_w is the energy source from the molten filler metal. S_q accounts for additional energy source and sink terms, e.g., the laser heat flux, convective heat losses, radiative losses, evaporation losses, and recondensation. To account for the spatial distribution, a refined ray-tracing approach was utilized considering multiple reflections of the laser radiation at the keyhole walls and Fresnel absorption. Many details of the numerical procedure, as well as the material parameters, can be found in the authors' recent studies.[19,20] Additionally, the model validation was shown many times for austenitic stainless steel AISI 304 as well as for the unalloyed steel.[10,11,19,20] Therefore, this part will not be repeated here once more.

IV. RESULTS

The comparison of experimental as well as numerical cross-sectional and longitudinal section weld pool sizes can be seen in Fig. 4. In Fig. 4(a), the upper part of the weld is dominated by the impact of the molten wire. In the liquid bridge transfer mode, additional heat was thus transferred into the upper weld pool area. Figures 4(b) and 4(c) show that the model can also predict the longitudinal size of the weld pool very well. Note that the results shown in Fig. 4(b) and the corresponding numerical result in Fig. 4(c) were done without additional filler wire. Here, an interesting aspect is the development of a narrow region just below the upper weld pool area, where the Marangoni stresses and the flow due to the recoil forces

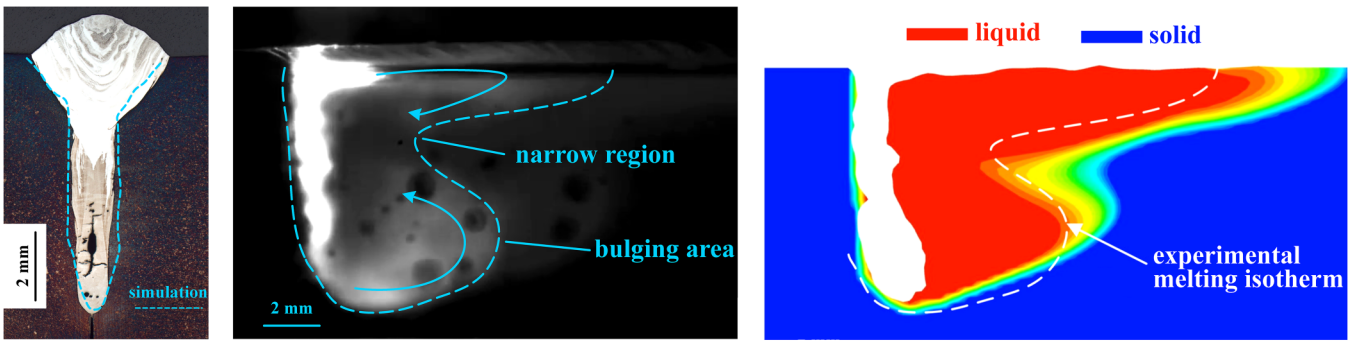

FIG. 4. (a) Comparison of the experimental and numerical cross sections of wire feed LBW of AISI 304 with an NiCr20Mo15 filler wire. (b) Longitudinal cross section and main flow routes using a setup of steel and quartz glass for optical inspection of the weld from the side during the process. (c) Comparison of the experimental and numerical longitudinal cross sections. Images (a) and (b) are taken and rearranged from our previous study (Ref. 21). Bachmann *et al.*, Adv. Eng. Mater. **24**, 2101299 (2022). Copyright 2022 Author(s), licensed under a Creative Commons Attribution (CC BY) license.

lead to an elongation of the melt pool. This was observed in numerous studies of LBW with and without wire support.[3,5,8,10] In current studies of the authors,[10,19,22] a distinct narrowing of the weld pool in its longitudinal section was observed. This can be seen in Figs. 4(b) and 4(c) as well. The shape of the weld pool can change with time even in quasistatic conditions. In Fig. 5, note the differently shaped weld pool extensions at different times during the welding process showing either a classical shape without a bulge at the early stage, Fig. 5(a), or a fully developed bulging and narrowing of the weld isothermal lines after reaching a quasistable state, Fig. 5(b). In both cases, the upper part is dominated by the Marangoni force, whereas the lower part is influenced mainly by the recoil pressure due to evaporation. In between, the recirculation flows of both areas combine a backflow in the direction of the keyhole leading to a narrow region with very short times between melting and solidification. In Ref. 10, the bulging phenomenon was justified as a result of the backflow at the weld pool surface due to the thermocapillary-driven flow. Moreover, a significant influence on the solidification behavior and finally on the hot-cracking susceptibility was postulated. Later, in Ref. 19, a critical minimum depth between 6 and 9 mm was found for the occurrence of the bulging, which agrees very well with the results of this study. Also note that the weld defect in Fig. 4(a) lies exactly in the region of the bulge. Here, solidification was delayed compared to the narrow region above. Premature solidification occurs because of the very short local weld pool lifetime and the

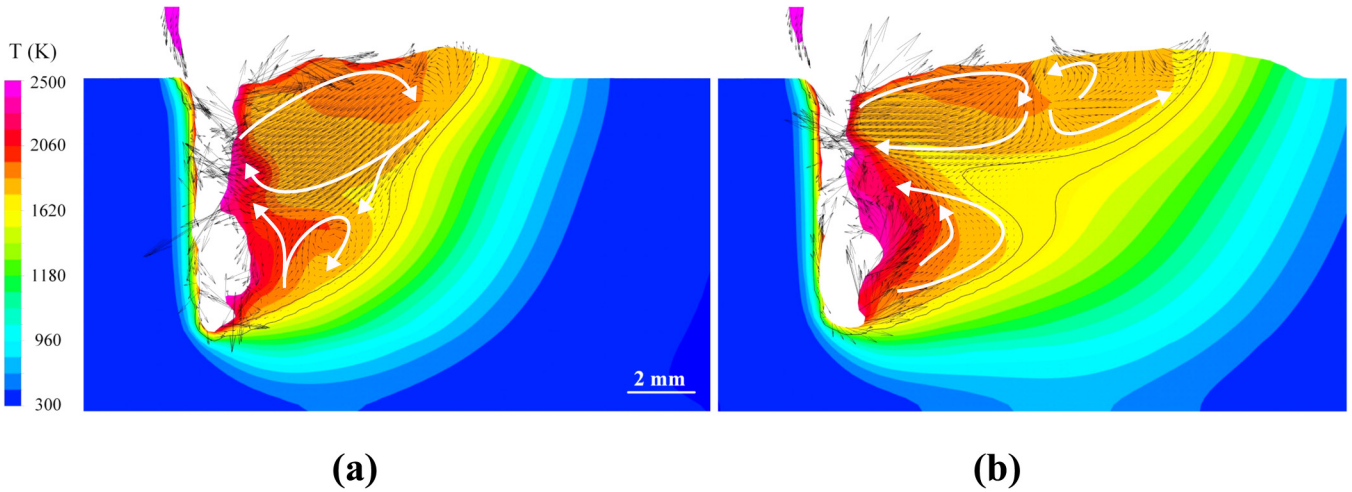

FIG. 5. Weld cross sections with main flow routes for the welding of AISI 304 with filler wire at different points in time showing differently developed bulging.

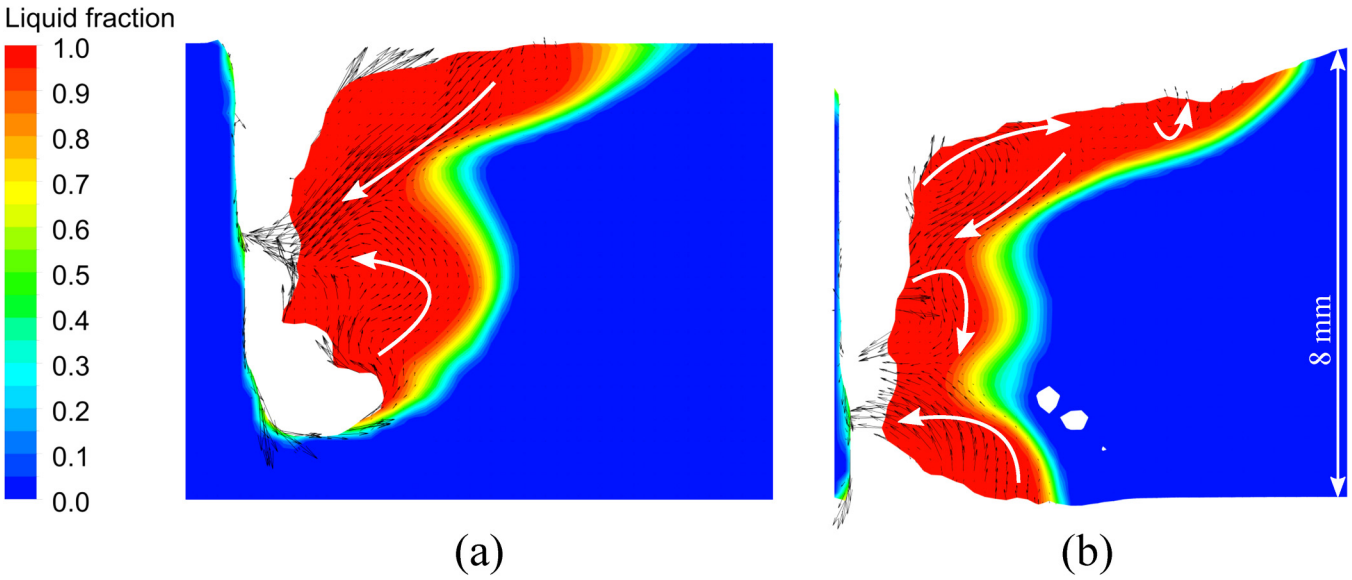

FIG. 6. (a) Weld cross sections with main flow routes for the welding of unalloyed steel S355 in partial penetration weld in a 12 mm thick plate (not fully shown here) and in a 8 mm full-penetration mode.

development of local tensile stresses during solidification that cannot be balanced by the remaining liquid metal. Similar behavior was also observed for partial penetration welding in 25 mm thick unalloyed steel S355.[22] This shows that this phenomenon occurs not only for austenitic stainless steel grades but also for low or unalloyed steel, see Figs. 6(a) and 6(b) for partial and full-penetration welds made of S355. The building mechanism of the bulge, and also the narrow region aside, is the same here as long as the critical minimum laser penetration depth was reached. This is in accordance with the current research.[8,23–25]

Another effect alongside the potential effects on the solidification behavior is the interference of the dilution of the filler material in the depth of the weld pool as the Marangoni-dominated regions of the weld pool and the lower part remain separated. Thus, the

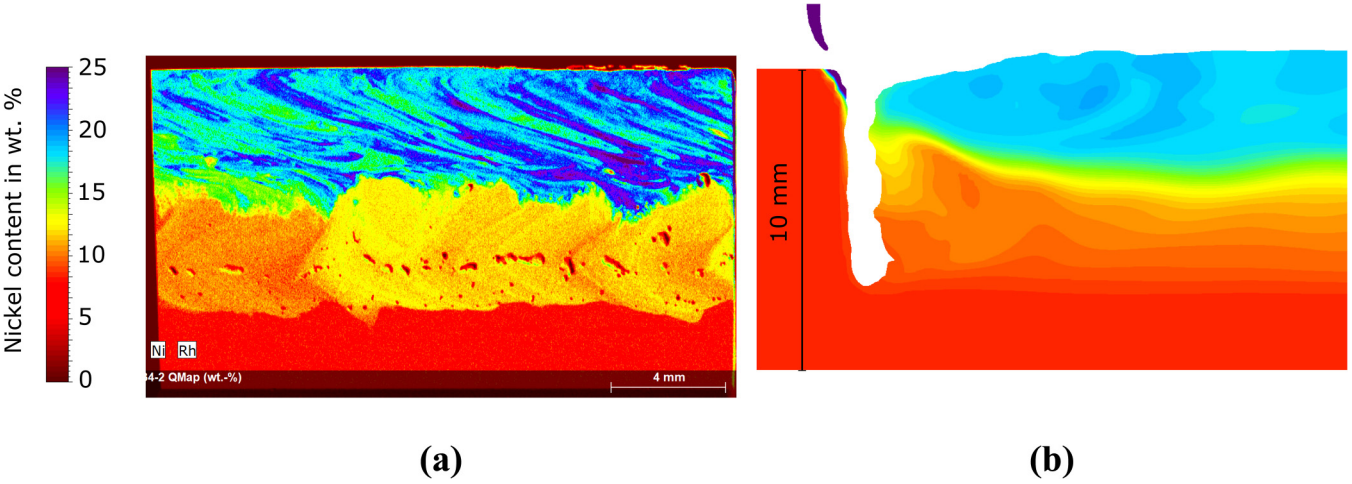

FIG. 7. Nickel distribution in the longitudinal section of wire feed laser beam welding of AISI 304 with an NiCr20Mo15 filler wire. (a) Experimental and (b) numerical results. Images are taken and rearranged from our previous study (Ref. 21). Bachmann *et al.*, Adv. Eng. Mater. **24**, 2101299 (2022). Copyright 2022 Author(s), licensed under a Creative Commons Attribution (CC BY) license.

wire material is trapped in the upper weld pool area, whereas the lower weld pool part remains dominated by the composition of the base material. This can be well seen in the XRF results in Fig. 7(a) as well as in the numerical simulation result for wire feed LBW of austenitic stainless steel AISI 304 with an NiCr20Mo15 filler wire in Fig. 7(b). Note here that the jump in the nickel distribution at around mid-depth of the weld pool corresponds exactly to the position of the narrow region shown in Figs. 4(b), 4(c) and 5(b). Consequently, the inhomogeneous distribution of the alloying elements added by the filler wire has a detrimental effect on the resulting mechanical properties of the weld.

The weld pool narrowing has another effect on the weld pool behavior and thus also on the resulting weld quality as the escape routes of the intrinsic keyhole-tip porosity are remarkably constricted. Hence, the process pores are captured by the solidification front before they can be lifted through the remaining vertical flow channel to reach the upper surface. In the end, the pores were frozen in the solidifying steel melt. Hereto note the longitudinal cross section of the partial penetration weld of AISI 304 steel in Fig. 8(a) with the distinct narrowing of the weld pool already known from Fig. 4(b) and the projection of the pores in the welding direction coming from μ-CT measurements as shown in Fig. 8(b). As highlighted, the bottom area containing most of the pores corresponds very well with the narrow region in the middle of the weld pool in both images. Kawahito *et al.*[4] report a velocity dependence of the ability of the pores to escape from the melt during the process. This in combination with the finding of a critical penetration depth for the development of bulging and a narrow region above supports the hypothesis of a mechanism keeping the pores trapped in the lower weld pool part. Instabilities at the keyhole tip are substantially responsible for the development of the porosity

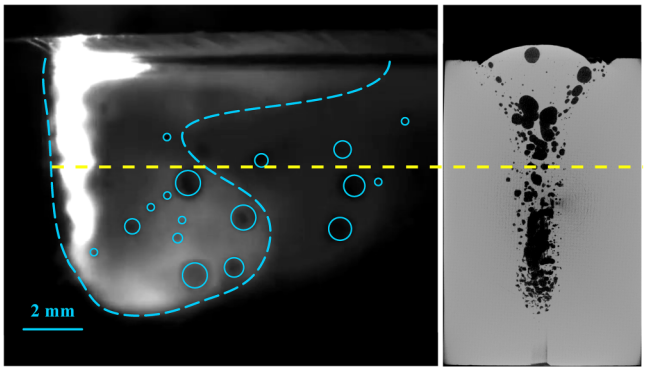

FIG. 8. (a) Longitudinal cross section and main visible porosity using a setup of AISI 304 metal and quartz glass for optical inspection of the weld from the side. (b) Projection of the porosity distribution on the weld cross section from μ-CT measurements. Note the weld pool bottom area below the yellow line where most of the pores are concentrated. Image (a) is taken and rearranged from our previous study (Ref. 21). Bachmann *et al.*, Adv. Eng. Mater. **24**, 2101299 (2022). Copyright 2022 Author(s), licensed under a Creative Commons Attribution (CC BY) license.

itself, and their potential ability to escape through vertical flow channels is obviously depending on the time to reach the weld surface. This can be longer for thicker welds and at the same time be negatively affected by the occurrence of narrow regions, which occur at higher penetration thicknesses. This is also in line with the study of Tan and Shin[26] relating the welding speed to different shapes of the keyhole. Additionally, it was reported, e.g., by Pang *et al.*[27] that rapid cooling at the keyhole surface can lower the vapor pressure inside the keyhole tip, which allows shielding gas to be entrapped easier in the melt as pores. Thus, in combination with the observed effect of a weld pool narrowing, the mechanism of the development of the process pores and their occurrence in the lower weld pool area observed here can be explained straightforwardly.

V. CONCLUSION

In the current study, numerical as well as experimental methods were utilized to investigate the narrowing of the weld pool, which occurs transiently during high-power LBW, and its consequences on resulting potential detrimental influences on the weld properties.

The main conclusions can be drawn from the results as follows:

- A distinct narrowing, sometimes accompanied by a bulge, can occur under the influence of pronounced recirculation zones at the free surfaces of the weld in the full-penetration mode, or even in the partial penetration mode, when a counterclockwise recirculation flow next to the keyhole-tip region is present as well.
- The nonuniform solidification behavior accompanied by the low resistance of the remaining liquid in the bulge against tensile forces during cooling leads to enhanced solidification cracking issues.
- The narrowing phenomenon has a direct influence on the flow routes into the weld pool, which causes a nonhomogeneous mixing of added filler wire metal, especially in the depth direction of the weld pool as the narrow region blocks the material transfer. This effect deteriorates the mechanical properties of the final weld.
- The closing effect of the vertical flow channels by the narrowing of the weld pool in its middle part leads to pores in the lower weld pool part that cannot escape to the upper weld pool surface. The counterclockwise recirculation zone observed in the lower weld pool part forces the pores to remain trapped and the solidification captures them accordingly.

ACKNOWLEDGMENTS

This work is funded by the Deutsche Forschungsgemeinschaft (DFG, German Research Foundation) Project Nos. 411393804 (BA 5555/5-2), 416014189 (BA 5555/6-1), and 466939224 (BA 5555/9-1).

AUTHOR DECLARATIONS

Conflict of Interest

The authors have no conflicts to disclose.

Author Contributions

Marcel Bachmann: Conceptualization (equal); Funding acquisition (equal); Investigation (equal); Methodology (equal); Project

administration (lead); Resources (equal); Supervision (lead); Visualization (equal); Writing – original draft (lead); Writing – review & editing (lead). **Xiangmeng Meng:** Conceptualization (equal); Data curation (lead); Formal analysis (lead); Funding acquisition (equal); Investigation (equal); Methodology (equal); Software (lead); Validation (equal); Visualization (equal); Writing – review & editing (supporting). **Antoni Artinov:** Conceptualization (equal); Data curation (supporting); Formal analysis (supporting); Investigation (supporting); Methodology (equal); Software (equal); Validation (equal); Visualization (equal); Writing – review & editing (supporting). **Michael Rethmeier:** Funding acquisition (supporting); Project administration (supporting); Supervision (equal); Writing – review & editing (supporting).

REFERENCES

[1]D. T. Swift-Hook and A. E. F. Gick, "Penetration welding with lasers," Weld. J. **52**, 492–499 (1973).
[2]M. Bachmann, A. Gumenyuk, and M. Rethmeier, "Welding with high-power lasers: Trends and developments," Phys. Proc. **83**, 15–25 (2016).
[3]S. Katayama, Y. Kawahito, and M. Mizutani, "Elucidation of laser welding phenomena and factors affecting weld penetration and welding defects," Phys. Proc. **5**, 9–17 (2010).
[4]Y. Kawahito, Y. Uemura, Y. Doi, M. Mizutani, K. Nishimoto, H. Kawakami, M. Tanaka, H. Fujii, K. Nakata, and S. Katayama, "Elucidation of the effect of welding speed on melt flows in high-brightness and high-power laser welding of stainless steel on basis of three-dimensional X-ray transmission *in situ* observation," Weld. Int. **31**, 206–213 (2017).
[5]S. Pang, L. Chen, J. Zhou, Y. Yin, and T. Chen, "A three-dimensional sharp interface model for self-consistent keyhole and weld pool dynamics in deep penetration laser welding," J. Phys. D: Appl. Phys. **44**, 025301 (2011).
[6]T. Shida, H. Okumura, and Y. Kawada, "Effects of welding parameters and prevention of defects in deep penetration electron beam welding of heavy section steel plates," Weld. World **17**, 196–207 (1979).
[7]S. Tsukamoto and H. Irie, "Mechanism of locally delayed solidification in electron beam welding," Weld. Int. **5**, 177–183 (1991).
[8]H. Wang, M. Nakanishi, and Y. Kawahito, "Dynamic balance of heat and mass in high power density laser welding," Opt. Express **26**, 6392–6399 (2018).
[9]Y. Feng, X. Gao, Y. Zhang, C. Peng, X. Gui, Y. Sun, and X. Xiao, "Simulation and experiment for dynamics of laser welding keyhole and molten pool at different penetration status," Int. J. Adv. Manuf. Technol. **112**, 2301–2312 (2021).
[10]A. Artinov, N. Bakir, M. Bachmann, A. Gumenyuk, S.-J. Na, and M. Rethmeier, "On the search for the origin of the bulge effect in high power laser beam welding," J. Laser Appl. **31**, 022413 (2019).
[11]X. Meng, A. Artinov, M. Bachmann, and M. Rethmeier, "Theoretical study of influence of electromagnetic stirring on transport phenomena in wire feed laser beam welding," J. Laser Appl. **32**, 022026 (2020).
[12]C. Panwisawas, B. Perumal, R. M. Ward, N. Turner, R. P. Turner, J. W. Brooks, and H. C. Basoalto, "Keyhole formation and thermal fluid flow-induced porosity during laser fusion welding in titanium alloys: Experimental and modelling," Acta Mater. **126**, 251–263 (2017).
[13]C. W. Hirt and B. D. Nichols, "Volume of fluid (VOF) method for the dynamics of free boundaries," J. Comput. Phys. **39**, 201–225 (1981).
[14]C. Prakash, M. Samonds, and A. K. Singhal, "A fixed grid numerical methodology for phase change problems involving a moving heat source," Int. J. Heat Mass Transfer **30**, 2690–2694 (1987).
[15]A. D. Brent, V. R. Voller, and K. J. Reid, "Enthalpy-porosity technique for modeling convection-diffusion phase change: Application to the melting of a pure metal," Numer. Heat Transfer **13**, 297–318 (1988).
[16]T. E. Faber, *Fluid Dynamics for Physicists* (Cambridge University, Cambridge, 1995).
[17]V. Semak and A. Matsunawa, "The role of recoil pressure in energy balance during laser materials processing," J. Phys. D: Appl. Phys. **30**, 2541–2552 (1997).
[18]K. C. Mills, B. J. Keene, R. F. Brooks, and A. Shirali, "Marangoni effects in welding," Philos. Trans. R. Soc. London, Ser. A **356**, 911–925 (1998).
[19]A. Artinov, X. Meng, M. Bachmann, and M. Rethmeier, "Study on the transition behavior of the bulging effect during deep penetration laser beam welding," Int. J. Heat Mass Transfer **184**, 122171 (2022).
[20]X. Meng, A. Artinov, M. Bachmann, Ö Üstündağ, A. Gumenyuk, and M. Rethmeier, "The detrimental molten pool narrowing phenomenon in wire feed laser beam welding and its suppression by magnetohydrodynamic technique," Int. J. Heat Mass Transfer **193**, 122913 (2022).
[21]M. Bachmann, X. Meng, A. Artinov, and M. Rethmeier, "Elucidation of the bulging effect by an improved ray-tracing algorithm in deep penetration wire feed laser beam welding and its influence on the mixing behavior," Adv. Eng. Mater. **24**, 2101299 (2022).
[22]A. Artinov, X. Meng, N. Bakir, Ö Üstündağ, M. Bachmann, A. Gumenyuk, and M. Rethmeier, "The bulging effect and its relevance in high power laser beam welding," IOP Conf. Ser.: Mater. Sci. Eng. **1135**, 012003 (2021).
[23]W.-I. Cho, S.-J. Na, C. Thomy, and F. Vollertsen, "Numerical simulation of molten pool dynamics in high power disk laser welding," J. Mater. Process. Technol. **212**, 262–275 (2012).
[24]H. Zhao, W. Niu, B. Zhang, Y. Lei, M. Kodama, and T. Ishide, "Modelling of keyhole dynamics and porosity formation considering the adaptive keyhole shape and three-phase coupling during deep-penetration laser welding," J. Phys. D: Appl. Phys. **44**, 485302 (2011).
[25]J. Powell, T. Ilar, J. Frostevarg, M. J. Torkamany, S.-J. Na, D. Petring, L. Zhang, and A. F. H. Kaplan, "Weld root instabilities in fiber laser welding," J. Laser Appl. **27**, S29008 (2015).
[26]W. Tan and Y. C. Shin, "Analysis of multi-phase interaction and its effects on keyhole dynamics with a multi-physics numerical model," J. Phys. D: Appl. Phys. **47**, 345501 (2014).
[27]S. Pang, W. Chen, and W. Wang, "A quantitative model of keyhole instability induced porosity in laser welding of titanium alloy," Metall. Mater. Trans. A **45**, 2808–2818 (2014).